Engineering Educators Bringing the World Together
2025 ASEE Annual Conference & Exposition
Palais des congrès de Montréal, Montréal, QC • June 22–25, 2025 ASEE
Paper ID #45724

DESIGN BUILD & TEST: A COST-EFFECTIVE & EFFICIENT 2X2 ANTENNA ARRAY - Numerical & Experimental Investigation

Dr. Cyril B Okhio P.E., Kennesaw State University

Cyril B. Okhio is a Faculty at the Southern Polytechnic College of Engineering & Engineering Technology, Kennesaw State University and an Adjunct Professor at Clark Atlanta University's Dual Degree Engineering Program. He earned his B.S. (Engineering) and Ph.D. (Mechanical Engineering) degrees from, and was an (Science and Engineering Research Council) SERC Post-Doctoral Research Fellow at the University of London. He is registered as a Chartered Professional Engineer (CPE) with the Council of Registered Engineers, United Kingdom; a Member of the Institution of Mechanical Engineers, UK and a Member of the Institute of Transportation Engineers, USA. Dr. Okhio has many years of administrative experience including Chairmanship of a Mechanical Engineering Department. Dr. Okhio understands that most engineering problems require multi-disciplinary solutions that embrace the new concepts of PLM approach so that the resulting solutions can be sustainable and all encompassing. Dr. Okhio has carried out experimental and numerical investigations of, and developed statistical analysis tools and computer codes, for the calculation of complex fluid flows. Some of this work has been published in international journals. He is currently involved in multi-disciplinary research and development concerning Condition Monitoring of Engineered Systems; applications of Additive Manufacturing Tools to the study of Design for Manufacturability of Engineering Components and Systems; Vehicular Systems and Safety Engineering, associated with SPSU Visualization & Simulation Research Center for which he is a co-PI. Dr. Okhio is very familiar with the level of technology and development, world-wide. He has visited many countries including Taiwan, Japan, Saudi Arabia, Zambia, Zimbabwe, Ghana, Senegal, Belgium, Germany, Austria, Italy, France, and he lived in the United Kingdom for more than 12 years. He is married with two children.

Dr. Theodore Orrin Grosch, Kennesaw State University

Dr. Grosch earned his BSEE in 1982, MSEE in 1987, and Ph.D. in Electrical Engineering at The Pennsylvania State University in 1993. He have worked at Hughes Aircraft, General Electric, M.I.T. Lincoln Laboratory two start-ups. Dr. Grosch has taught at Univ

Dr. Austin B. Asgill P.E., Kennesaw State University

Dr Austin B. Asgill received his B.Eng.(hons) (E.E.) degree from Fourah Bay College, University of Sierra Leone, his M.Sc. (E.E.) degree from the University of Aston in Birmingham, and his Ph.D. in Electrical Engineering from the University of South Florida. He is currently a Professor of Engineering Technology (Electrical) at Kennesaw State University (KSU) and has previously served as Department Chair of Electrical and Computer Engineering Technology (ECET). Prior to joining the faculty at KSU (formerly SPSU), he was an Associate Professor of Electronic Engineering Technology at Florida A&M University (FAMU), where he served as Program Area Coordinator and Interim Division Director. With over 30 years of teaching experience in Electrical/Electronic Engineering and Engineering Technology, he currently teaches in the areas of networking, communication systems, biomedical instrumentation, digital signal processing, and analog and digital electronics. He has worked in industry in the areas of telephony, networking, switching and transmission systems, and RF and MMIC circuits and system design. Dr. Asgill also has an MBA in Entrepreneurial Management from Florida State University. He has served on the board of the Tau Alpha Pi (TAP) National ET Honors Society since 2012 (Chair 2012-2014). He is a Life Senior Member of the IEEE, a Member of the ASEE, and is a licensed Professional Engineer (P.E.) in the state of Florida.

Saiyda N Bey

Helical Antenna Array for High Boresight Gain

Introduction

Since the early 1900s and the birth of wireless communication, antenna design has been an integral field to electrical engineering. Antennas are the primary component in wireless radio frequency communications, converting alternating current moving through a conductor and radiating that energy in the form of electromagnetic waves. In an ever-growing wireless world, improvements and new antenna designs are pushing the ceiling with what can be achieved even using simple materials to construct an antenna.

This project aims to develop a high-gain helical antenna array targeting 20 dBi at 2.4 GHz. The goal is to achieve a narrow, focused beam and maximize gain along the boresight axis, enabling reliable long-range and precise communication. To achieve this, the project will require careful consideration of material conductivity, permittivity, cost, and physical limitations like size and wire spacing. A simulation model is to be created and compared with real-world testing using KSU's StarLab and VNAs as well as testing at Microwave Vision Group's NIST certified SG64 antenna measurement system (MVG).

A significant challenge lies in balancing individual element gain with phase synchronization. While achieving the desired gain per element is crucial, their radiation phases must also align for a perfectly combined signal. This necessitates meticulous adjustments to wire lengths to achieve near-perfect phase matching. The project prioritizes high boresight gain, large bandwidth, and simplicity using materials and parts that are readily available from a hardware store or online. While helical antennas offer high individual gain, their inherent relationship between larger size and higher gain invites inconsistencies in element length and therefore phase as the helix is made ever-longer. Utilizing multiple lower-gain elements presents its own challenge, as it increases the complexity of managing phase-differences by requiring a complex feed network that will never be perfectly phase-balanced. Additionally, complex feed networks for many elements can significantly increase costs. Because of these trade-offs, a low overall volume with fewer elements was targeted, leveraging the natural bandwidth of higher-gain uniform helices. This approach was selected to achieve the desired performance while maintaining a cost-effective and compact design.

Another advantage of the choice of helical elements is their inherent circular polarization. The 20dBi boresight gain target is quite high, unnecessarily high for most terrestrial point-to-point communications. Gain of these levels is, however, common for satellite communications as are those that utilize circular polarization due to their hand-switching reflections that mitigate the effects of reflective and imperfect signal paths. Ultimately, the frequency of 2.4GHz was chosen for its commonality and ease of comparison with other designs from teams with lower access to sophisticated measurement equipment. The helical antenna was chosen for its easy scaling for different operating frequencies, meaning that this design could be translated for use in the L-band or other based on practical use case. With a focus on good design, validation, and measurement practices, this design and its production processes can serve as a reference for similar designs in the future teams.

Review of Literature

To gain a comprehensive understanding of Boresight Gain Wire Antenna Arrays, recent research articles were reviewed. These studies examined different design techniques and their effects on the performance of arrays.

This project involves optimizing antenna performance for Wi-Fi applications in the 2.4 GHz frequency range. The article explores feeding arrangements, reflector modifications, and gain improvement through simulation and notes their performance as: gain. S11, and beamwidth. This will be useful to choose the best radiating element. [Source I]

This article examines the difference between a traditional horizontal and an inverted V dipole. The paper notes the signal-to-noise ratio and the widening of the radiation pattern. The results show using the inverted V dipole with the increase in the signal-to-noise ratio at 45 degrees from boresight. [Source II]

Array antennas can be used for a variety of circumstances and be built with a wide range of elements. This article discusses how the structure and elements of an array can change to performance and affect the beam in terms of phase and amplitude. Results can be seen from testing and models provided in the paper. [Source III]

Linear array antennas are comprised of multiple identical elements and are carefully positioned in a particular arrangement. This article discusses the testing of a linear array with evenly distributed distances with differing elements. The antenna was tested using the quadratic Koch curve, which is a fractural curve, and the performance was evaluated. [Source IV]

Wire grid array antennas can be built in many ways with many different materials. This article discusses the design, simulation, fabrication, and testing of a low-cost antenna using foam as a ground plane and copper as a conducting material. When this antenna was tested, the reflection was shown to be –11.44 dB. [Source V]

Wire grid array antennas are manufactured or fabricated. This article discusses a unique design of a wire grid array antenna by etching lines into a certain number of loops on a dielectric sheet backed by a metallic ground plane. The results of this study showed good gain, bandwidth, and cross polarization properties. The etching method proves comparable to conventional methods. [Source VI]

Grid array antennas are elements of linear polarization, this antenna is fed using a coaxial line in the center as opposed to side feeding. The current distribution was shown to be almost symmetrical. This design showed a 62% reduction in overall area with a 6.4% drop in gain. [Source VII]

This article discusses a wire grid array antenna designed with parasitic monopoles for changing beam polarization without affecting the radiation pattern. The polarization transformer alters the beam's polarization to linear or circular. The circularly polarized beam was almost symmetric with respect to the antenna axis. [Source VIII]

A low-cost antenna-pattern measurement system was developed using software-defined radios (SDRs) and open-source hardware. The paper discusses methods used to calculate gain and

other antenna characteristics from measured data. Hardware and software tools discussed could help inform strategies used for the WGA antenna design, build, and test. [Source IX]

Designs, characteristics, and applications of crossed dipole antennas were presented, with specific discussion on dual feed crossed dipoles and their versatility. Recent developments of single-feed designs were explained, with emphasis on how techniques like division of dipole arms and utilization of meander lines can allow for miniaturization, bandwidth enhancements, and radiation pattern control. This information on crossed dipole antenna design techniques will aid in the conceptualization and design of the WGA antenna. [Source X]

Changing patterns with an antenna, switches are typically used to do that, but with the disadvantage of one cannot alter the radiation pattern of the antenna. This article covers the process of creating an antenna where they can reconfigure the pattern without the downsides using different methods involved in beam steering. It explains the design process, as well as the results behind each test comparing it with past designs that did not operate as smoothly as this. [Source XI]

Depending on where an antenna is fed, the direction of the linear polarization can be altered. When fed from the edge it can have a tilted beam while when it's fed from the center the wave is in the direction normal to the array. This article goes over how changing elements on the antenna itself can change the polarization of the radiation it emits. The addition of loop elements in an array instead of a linear element changes the radiation of the antenna from linear polarization to circular polarization. The gain also increased from this change. [Source XII]

Having an antenna which is matched for a wide range of frequencies is important since a single antenna can be used for multiple applications. This can be done by having a wide bandwidth which also helps keep the antenna functional in a specific frequency if there are any manufacturing errors and the resonant frequency is shifted. A sturdy dipole antenna is examined in this article which has a large bandwidth and an isotropic radiation pattern. [Source XIII]

A loop antenna provides a very isotropic radiation pattern however they are not automatically matched with a 50-ohm source and thus a matching network must be implemented. In this paper, a loop antenna is matched with a 50-ohm source without a traditional matching network and instead uses gaps in the loop antenna to change its resistance without affecting its resonant frequency. A 3D model of the antenna was created and simulated in CST (EM simulation software) and a physical prototype was also later created to verify the simulated results. [Source XIV]

Antennas can be many different shapes or have several feed lines. The effect of the antenna shape can be seen in the antenna's range of beam and efficiency. In this paper, the experimental antenna shape was rhombic. The results concluded with the Rhombic Grid Array

Antenna having a greater radiation efficiency when compared to a standard grid array antenna. [Source XV]

This article shows an example of a designed and tested copper wire antenna with 2.4GHz band operation. The dimensions of the copper wire are 40 mm x 5 mm and is being fed by a 50-ohm coaxial cable 30mm in length. This copper wire antenna can be fine-tuned by adjusting the length of the shorter radiating element. [Source XVI]

The antenna design textbook provides detailed information on various types of antennas and the mathematical principles required to develop a functional model. It covers both theoretical concepts and practical aspects of antenna design, essential for the entire process from design to testing and construction. Chapter 5 offers specific examples of Dipole/Monopole antennas along with a section dedicated to Antenna Arrays, which serve as valuable resources for facilitating the design process. Additionally, Chapter 6 presents analyses and examples focused on Wire-type Antenna designs, further enriching the understanding and application of antenna theory and practice. [Source XVII]

Increasing the range of antennas efficiently is often challenging. In this paper, the experiment aimed to implement and compare the performance of conventional Wi-Fi routers with those using directional antennas. The results indicated that directional antennas enhanced performance compared to conventional non-directed antennas. [Source XVIII]

The capacity growth of antenna arrays with multiple antennas operating at 1.9 GHz was simulated and analyzed using WiSe, an experimental ray tracing tool, across various operating environments. The study observed higher signal-to-noise ratio (SNR) and capacity when the transmitting and receiving antenna arrays were spaced up to 3 wavelengths (λ) apart. [Source XIX]

The paper characterizes traditional antenna design methodology as "exhaustive" and asserts its lack of guarantee in yielding successful outcomes due to the complexity of modern antennas. It presents examples showcasing the benefits of employing machine learning-assisted antenna optimization to ensure comprehensive optimization across numerous antenna parameters. Furthermore, the paper delineates the disparity between single and multi-objective optimization methods in antenna design strategies. [Source XX]

The shape of radiating elements in an antenna significantly influences the radiation pattern and gain. In this paper, the experiment employed four configurations—two hexagonal and two rectangular—each comprising sixteen elements in a phased array of circular microstrip antennas. The results indicated that each configuration produced distinct beam patterns and levels of gain. [Source XXI]

There exist various methods for enhancing the gain of an antenna. In this paper, the experiment aimed to employ a novel shape and algorithm to design a microstrip antenna capable of achieving higher gain and broader bandwidth. The results demonstrated that the

microstrip antenna developed using the unique shape and algorithm exhibited both higher gain and broader bandwidth compared to a conventional microstrip antenna. [Source XXII]

The input impedance of an antenna can vary significantly depending on factors such as design considerations and the materials it's constructed with. This paper discusses a method for creating antennas that can be directly matched to the input impedance of various circuits by adjusting the width and length of the arms of the dipole. This approach eliminates the need for creating a new matching network, offering a more versatile and efficient solution. [Source XXIII]

LPDA (Log Periodic Dipole Arrays) as a reflector antenna feed offers a wide range of applications. However, phase center of the LPDA changes depending on the operation frequency, which, in turn, leads to defocusing loss as frequency changes. In this study, the design of 1-18 GHz printed LPDA antenna is used as a linearly polarized feed for the parabolic reflector which has a 1.2 m diameter. Optimal feed position and f/D ratio are chosen through extensive simulations. Performance parameters such as VSWR, gain and half power beamwidth are presented. Minimum aperture efficiency was recorded as 0.27 at the target band. [Source XXIV]

This resource discusses various operating principles of different types of antennas that can be utilized and incorporated into the design of a wire grid array antenna. Specifically, plane, corner, curved front-fed, and curved Cassegrain fed reflectors are described. There are recommended design specifications in the book that will assist in the project. [Source XXV]

This paper presents software for the automated design of parabolic reflector antennas. The software enables quick antenna design and evaluation of electrical characteristics. The method of moments is used to calculate feed radiation pattern with MATLAB Antenna Toolbox. The developed program allows users to choose feed as a horn, a dipole or turnstile antenna with reflector or a helical antenna. The program can be used to design front, offset or dual reflector (Cassegrain or Gregorian) antennas. It also calculates the radiation patterns of feed and overall antenna, and the field distribution in the antenna aperture. [Source XXVI]

The ME dipole is well known for its wideband performance, low cross-polarization, stable gain, and symmetrical radiation patterns in both E- and H- planes. Dual-polarized ME dipole antennas are widely used in base station systems as they provide polarization diversity along with the inherent advantages of ME dipole. They increase the channel capacity and aid in reducing the effects of fading caused by signals traveling over many pathways. [Source XXVII]

In this paper, a compact monopole antenna is presented for wireless local area network (WLAN) applications. The proposed structure consists of a quarter-wavelength monopole, a ground plane, and an annular sleeve. The sleeve and the ground plane form a quarter-wavelength cavity. The open-ended cavity increases the radiation aperture and enhances the antenna gain. A small piece of substrate is used to support the monopole and match the input impedance. The simulated and measured results agree well. [Source XXVIII]

Impedance mismatches in RF networks cause reflection which leads to power loss and poor signal to noise ratios. Both narrow and broadband matching techniques such as quarter wave transformer, taper lines, stubs, and lumped elements are covered in this resource. [Source XXIX]

The conditions for maximum power transfer from a source antenna to a receiving one are examined when the two antennas are close by. As an example, computed and measured results are described for the power transfer efficiency for two-element Yagi antennas. These results can be used to design matching networks between the antenna and a load such as a voltage multiplier for power transfer in a wireless sensor network. It is concluded that maximum PTE could be obtained by continuously tuning the antenna and matching network as the antenna separation and load conditions change. [Source XXX]

This article corrects misunderstandings about helical antennas, especially concerning the ideal impedance, and introduces a new data-based design method based on detailed simulations. The approach addresses practical considerations like conductor thickness and introduces a simple matching technique. Overall, the research aims to replace outdated design rules with a data-driven design set based on practical simulations that enhances helical antenna performance. [Source XXXI]

From conception to design to measurement and validation, this book contains a wealth of knowledge on antennas. For this project it contains relevant design parameters and theory for helical antennas. Parameters like circumference, element pitch, turns number are characterized using familiar parameters like wavelength or given bounds for different operating modes for the helix. It relevantly discusses the Axial Mode of operation for helices and the design equations around them. [Source XXXII]

Wang et al introduces a new method for analyzing the radiation characteristics of quadrifilar helix antennas, proposing a novel concept of multi-arm helix antennas. This method equates the quadrifilar helix antenna to a circular array antenna composed of four helix antennas, enabling the study of the radiation patterns and polarization characteristics of various multi-arm configurations. The analysis reveals that multi-arm helix antennas, when having more than two arms, exhibit similar radiation patterns and polarization characteristics. These patterns include a wide beam, a wide 3 dB axial ratio radiation pattern on the meridian plane, and an omnidirectional radiation pattern on the equatorial plane, with the trifilar helix antenna showing superior performance in terms of non-circularity and axial ratio. [XXXIII]

Description of the Approach

The approach decided for this project aims to achieve the 20 dBi gain by using four, 10-turn, helical elements for higher individual directivity over dipoles; greater ease in building and redundancy were also taken into strong consideration. Two helical antennas will be first be constructed, one using a coil made of enameled copper wire and the other of bare copper wire. Both antennae will be tested in the KSU StarLab to determine the effect (if any) of the enamel on the RF properties and tuning. Designing, tuning, and iterating the single-element performance is of paramount importance for this array, and repeated testing is needed to solidify this design

before moving on. After the testing has been conducted, the more promising array will be constructed using the aluminum ground plane as a mounting surface. Each antenna will be fed by a Wilkinson 1-to-4 Power Splitter chosen based on advertised low path loss and consistent phase between paths. This array will then be tested in KSU's StarLab antenna measurement system). Once the proper data has been gathered, reviewed, and discussed, optimization of the array can take place, as well as the testing opportunity at Microwave Vision Group's NIST Certified antenna measurement system to achieve boresight gain results with a quantified uncertainty.

Components

- 3D PLA Material
- 3D Support Structure Models
- 16-guage Copper Wire
- Copper Matching Strips
- 4 to 1 SMA Power Splitter/Combiner
- SMA Bulkhead Connectors
- SMA Cables
- Aluminum Ground Plane
- Acrylic Sheeting to protect ground plane and feed network

Design

The design process began by reviewing relevant antenna literature and the standards set by the prompt. After sharing and discussing findings, it was decided that the array design would utilize helical antennas due to their high gain and directivity which is maximum in the +z axis, as well as their inherent circular polarization. To achieve these characteristics, the helix antenna sacrifices any isotropic properties. The next step, choosing both the materials for the antennae and the ground plane, is essential. The prompt calls for single strand 16-Gauge AWG copper wire as the conductor material for the physical antennas, this was followed and enameled wire was also considered for its anticorrosive properties. In terms of the ground plane, it was determined by the team that aluminum was the best choice of ground plane due to its availability and low density compared to steel. Aluminum is also more conductive than steel, making it a better reflector of RF energy. The prompt suggested using Styrofoam as a reflecting plane however, this would not have provided a good mounting structure, nor would it have the same conductive effectiveness as aluminum.

In the next phase, helical antennas were further researched to determine what parameters most influenced their design. Design properties to create an antenna and descriptions of how each were utilized follows, starting with the given prompt frequency of 2.4 GHz:

- Wavelength [λ] – The length of the wave of the signal, where c is the speed of light and f is the prompt frequency
    - $\lambda = \frac{c}{f} = \frac{3*10^8}{2.4*10^9} = 125\ mm$
- Circumference [C] – The circumference of a turn on the helix antenna

    - Note that for a helix to operate in Axial Mode (signal traveling in one direction) antenna circumference must be near wavelength of operation: $\frac{3}{4} < \frac{C}{\lambda} < \frac{4}{3}$
    - This calculation results in a range of possible circumference choices. The most promising simulations occurred around a value of C = 125mm
- Diameter [D] – The diameter of a turn on the helix antenna
    - $D = \frac{C}{\pi} = \frac{125mm}{\pi} = 39.8\,mm$
- Vertical Separation [S] – The vertical distance between turns on the helix antenna
    - $S = 0.2 * C = 0.2 * 125\,mm = 25\,mm$
      where 0.2 is a standard value multiplied to assist with impedance matching in the design

- Pitch Angle [α] – Angle of how far helix dimensions increase in the z – axis
    - $\alpha = 13°$ was chosen because standard helix antennas function best between an angle of 12-14 degrees

- Number of Turns [N] – The number of complete turns made by the helix antenna
    - N = 10 turns
- Height [H] – The total height of the antenna
    - $H = N * S = 10 * 125\,mm = 1250\,mm$
- Length [L] – The total length of the conductor
    - $L = \sqrt{S^2 + C^2} * N = \sqrt{(125mm)^2 + (25mm)^2} * 10 = 1274\,mm$
- Conductor Diameter [d] – The diameter of the copper wire
    - $d = 1.29\,mm$
- Estimated Input Impedance [Z] – The estimated input impedance of the antenna
    - $Z = 140 * \frac{C}{\lambda}$
- Estimated Antenna Gain [G] – The estimated gain of one helix antenna
    - $G = 11.8 + 10\log(NS) = 11.8 * 10\log(10 * 0.125) = 18.7$ dBi

Using the calculations a simulated design of the antenna was created using Ansys HFSS software. The ACT Extension in the HFSS software contains an antenna wizard that makes creating any antenna much easier. The measurements required were the diameter, spacing, number of turns and the conductor's diameter. After entering the data HFSS generates a helical antenna design with associated ground plane and port shown in figure 1 below.

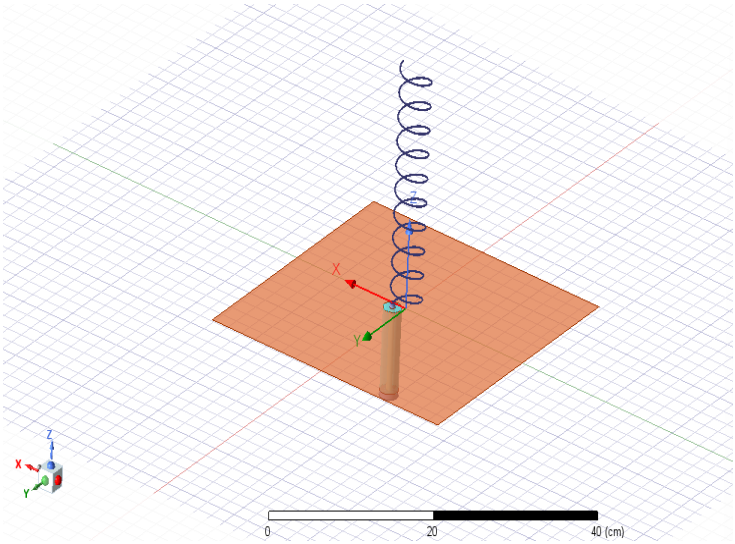

Figure 1 HFSS Antenna CAD Simulation

Once the model was created, various iterations took place to determine the most effective combination of the dependent variables with respect to the total gain of the antenna. The simulation parameters were set to sweep the frequency and test the antenna properties from 1.7 GHz to 3.0 GHz. These variables included the number of turns and the spacing between each helix as indicated by the estimated total gain equation. The circumference is also in the equation but because of the frequency requirement of 2.4 GHz, the circumference could not be modified. S11 return loss simulation data was gathered on each iteration of the test. During research it was determined that as N increases the gain also increases. This was used to set values of N to simulate however, values of N over 16 would reach a cutoff where the increase in gain would plateau. Any N values under 5 were undesired since the antenna will fall out of axial mode. N = 5, 8, 10, 12, and 16 were chosen and simulated. S11 data at N=10 was found to have the most even gain over a spread of frequency spectrums, this led to 10 turns being the chosen number for the project. Associated figures in the Results section show the different S11 data from the associated simulations are shown below:

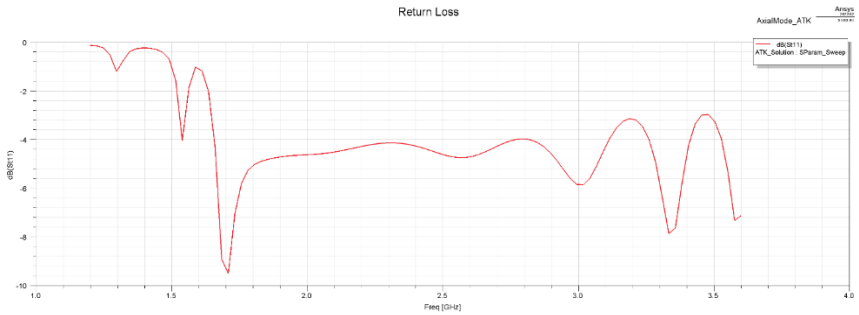

Figure 2 - 5- Turn S11 HFSS Simulation Results

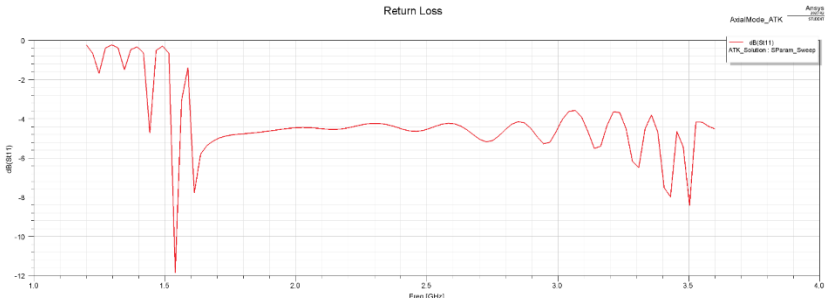

Figure 3- 8-Turn HFSS Simulation S11 Results

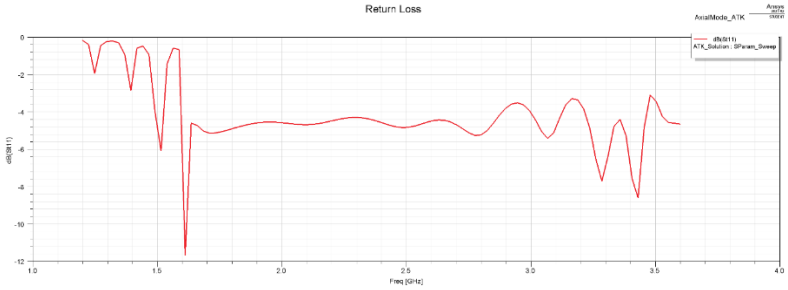

Figure 4 - 10-Turn HFSS Simulation S11 Result

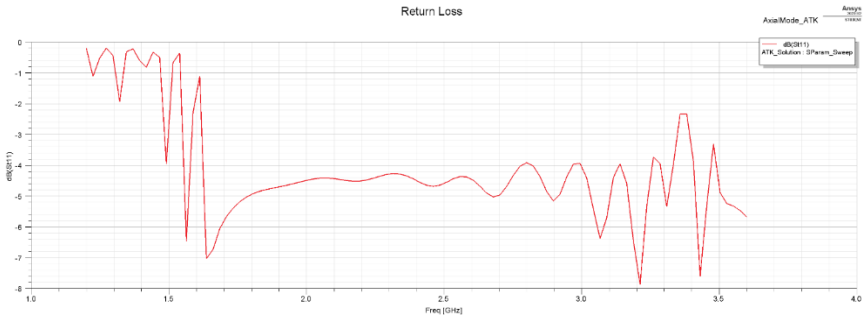

Figure 5 - 12-Turn HFSS Simulation S11 Results

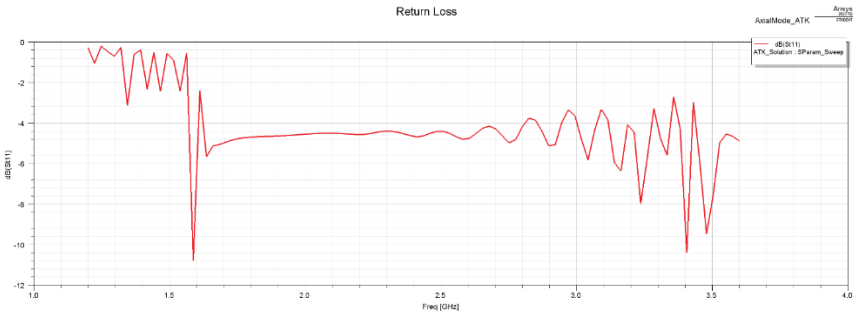

Figure 6 - 16-Turn HFSS Simulation S11 Results

Along with the S11 return loss plots, 3D beam plots were also acquired from the simulation. From these simulations gain estimations were given and can be viewed in the 2D far-field plot below:

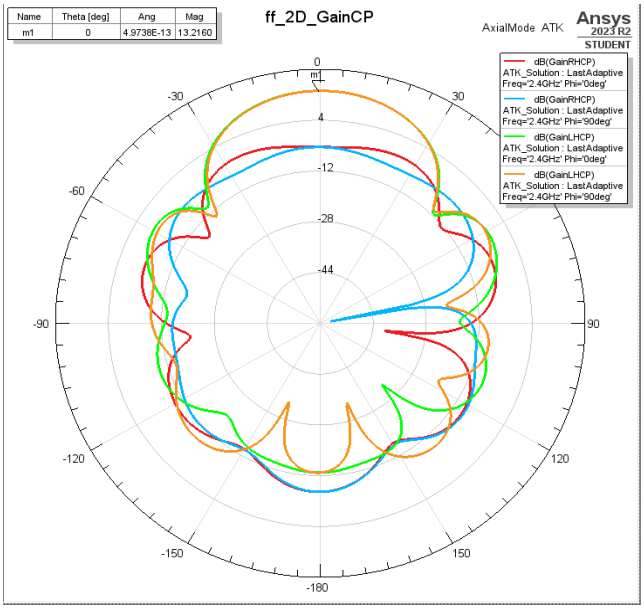

Figure 7 Far-Field Gain, N=10 turns

Reviewing the far field plots gave an estimated gain of around 13 dBi, which would be scaled up with the inclusion of more antennas to form the array. After the plots were reviewed and the dependent spacing and number variables were locked in the element was ready for construction. Holding the antennas in the right place to their correct specifications was the next challenge. Existing code for 3D printable support structures to hold the helix antennas in their proper places was acquired and edited to the specifications of the designed helix. An Ender V3 printer loaded with PLA filament was used to create the first iteration of the supports. Before the copper wire could be wound into the support structure a sort of pre-winding was required. Based on the helix circumference of 39.8 mm (roughly equal to 1.5 inches) a PVC pipe with similar dimensions was acquired to crudely prewrap the wire around so that it would thread well into the supports. The initial printing was successful, but problems were quickly identified. The conductor support holes, while smaller than the diameter of the conductor, would not support the process of winding the copper wire through them without damaging the uniformity of the coils themselves. A second iteration was attempted, increasing the size of the holes from 1.5 mm to 3

mm. This correction was a success, and the first coil was wound into its support structure. The figure below shows the antenna after winding:

Figure 8 Single Helix, wound into Support Structure

From here the wound conductor inside the support structure was mounted to the aluminum ground plane and an SMA connector was soldered to the feed end of the antenna. The single helix was then taken to the KSU electromagnetics lab where a VNA was used to measure the input impedance to determine the method of impedance matching that would be used on the antenna. It was determined that the most cost effective and reliable way to match the antenna would be a copper strip soldered near the antenna feed. This copper strip would run parallel to the ground plane with dimensions calculated to serve as a quarter-wavelength impedence transformer to match the roughly 140 ohm intrinsic impedence of the helix to the 50 ohm input impedence. After this matching process, this first helix's boresight gain saw an improvement from 8.7dB to 12.7dB, over a 2x improvement and near-enough to simulated results to determing that the enamel had little-to-no effect on the gain potential of these helices.

Once the impedance matching was completed, the antenna construction was replicated 3 more times to form a 2x2 helical antenna array. A 4-to-1 Wilkinson Power Splitter/Combiner was utilized to combine the 4 signals from the array into one feed and SMA cables were placed in a way that minimized sharp bends or corners, hand tightened, and tucked into place. Minimizing bends and sharp turns in an SMA cable is important to reduce the impact of any losses incurred from the length of the cable itself. A per-path attenuation of 0.7dB - 1.3dB was measured for this feed network, within the datasheet's specifications of the splitter with the cables included. Once assembled, 3D printed "feet" were added to the side of the ground plane opposite the antenna. A transparent acrylic sheet was then added to protect the feed points, SMA configuration, and the

mounted 1-to-4 power splitter. The following figure shows the completed antenna array, fully assembled:

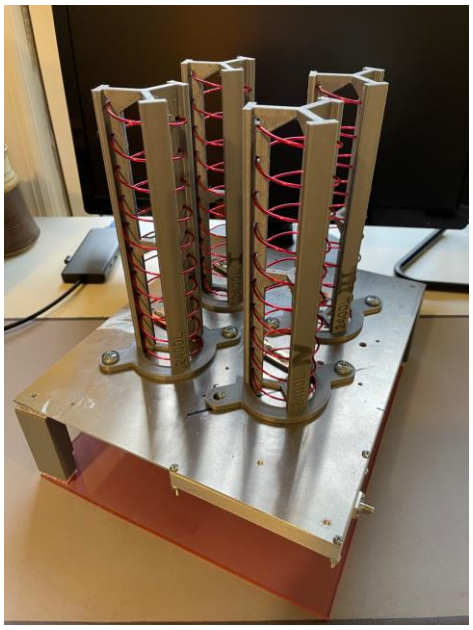

Figure 9 Fully Assembled Antenna Array

Experimental Results and Discussion

Results for this antenna were gathered across multiple systems, KSU's VNA's for return-loss measurements, KSU's StarLab for radiation patterns and associated data of the single element and full array validations, and MVG's NIST certified SG64 for final measurements. The results in this section will be arranged and discussed in the order that best suits antenna development, not necessarily the order in which they were acquired. Note that many tests can be performed in different orders with equal validity if the AUT remains unaltered between tests. Descriptions of each type of result will be discussed as well.

The first measurement to be conducted for any antenna is an S11 or return loss measurement. This measures the portion of power that is reflected at the feed-point of the antenna and is measured in dB. This same measurement can also be used to quantify the characteristic impedance of the antenna in a Smith Chart format. The first helices assembled, one with enameled wire and one bare, were mounted to the ground plane and suspended with foam, directed towards RF absorber to minimize the impact of reflections. The return loss results here were approximately –3.6dB, expected results for an un-matched antenna, corresponding to nearly half of sent power being reflected. The intrinsic impedance was measured to be approximately 17 – 40j ohms, found later to be an anomalous result through further research. These results were consistent between enameled and bare copper wire.

Figure 10 Return loss measurement setup

Research showed that the established approximation for a monofilar, axial mode helix is 140 * C/lambda with a negligibly small imaginary component. These helices were constructed such that C = lambda, so the experimental results differed greatly from theoretical. This indicated an error in the setup, probably with the torque of a connector or adaptor. With little time, it was decided to design matching strips around the theoretical 140-ohm impedance, which proved to be the correct choice. The first enameled-wire helix had significantly improved after matching and the following results were acquired at 2.4GHz.

Return Loss: ~-12dB

Intrinsic Impedance: 72.65 +j39.92 ohms

Boresight Gain @ 2.4GHz (measured in StarLab): 12.7dB

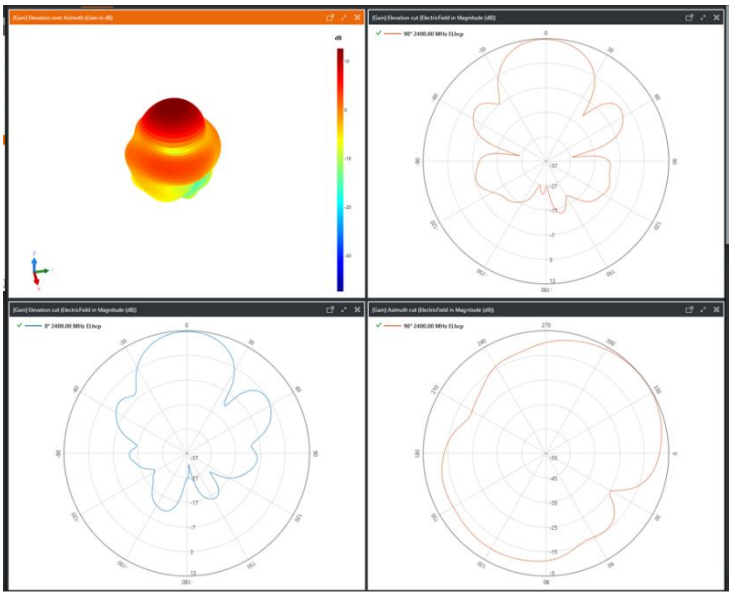

Figure 11 Radiation Pattern Measurements for Single Helix

This marked the largest stepping-stone for the design process. The 12.7dB boresight gain was very close to the simulated result, indicating that this composition of enameled wire and matching strip was an acceptable design to reproduce for the array. The team proceeded to construct, and measure return losses for these helices with the return loss target being less than –10dB (less than 10% of power reflected). Below are the measured results for each element at 2.4GHz, numbered radially starting from the one closest to the RF power splitter.

Element 1:

Return Loss: -11.12dB

Intrinsic Impedance: 59.59 +j29.82 Ohm

Element 2

Return Loss: -12.63dB

Intrinsic Impedance: 44.81 + j22.22 Ohm

Element 3

Return Loss: -10.058dB

Intrinsic Impedance: 72.65 + j32.92 Ohm

Element 4

Return Loss: -11.25dB

Intrinsic Impedance: 70.20 + j27.13 Ohm

As the antenna was ready to be constructed, the individual SMA feed cables and necessary adaptors were affixed to the RF power splitter and the assembly was mounted to the aluminum ground plane. From here, path losses could be characterized in this feed network by taking S21 measurements on KSU's VNA. Those results are tabulated below with the path number corresponding to the element number fed by that path.

Path 1 - Attenuation: 1.32dB

Path 2 - Attenuation: 0.86dB

Path 3 - Attenuation: 0.69dB

Path 4 - Attenuation: 0.70dB

Even including the cables, these results are within the <1.6dB attenuation noted on the power splitter datasheet. These losses directly impact the total gain of each associated element and therefore the full array.

Now that all parts of the array had been acquired or constructed, the full device could be assembled. After doing so, the array was measured in KSU's StarLab with boresight gain of 13.6dB at 2.4GHz and efficiency of around 70%. This measurement was later found to be inaccurate due to low torque on the antenna feed connections. These connections were tightened, the device reassembled, and the full array was measured in MVG's SG64. Below are the measured results including total gain and LHCP gain from Phi = 0 degrees.

Table 1: Tabulated Gain Results for SG64 Measurement

Frequency	Max Total Gain	Position	HPBW	Max LHCP	Position	HPBW
1700(MHz)	6.33 dB	3.80 deg	42.05 deg	0.78 dB	1.00 deg	41.76 deg
1725(MHz)	12.40 dB	1.20 deg	38.84 deg	11.96 dB	1.40 deg	38.39 deg
1750(MHz)	13.10 dB	1.20 deg	37.51 deg	13.05 dB	1.20 deg	37.31 deg
1775(MHz)	13.43 dB	-0.20 deg	36.87 deg	13.41 dB	-0.20 deg	36.35 deg
1800(MHz)	13.52 dB	0.20 deg	36.95 deg	13.42 dB	-0.20 deg	36.54 deg
1825(MHz)	13.63 dB	0.00 deg	35.72 deg	13.54 dB	-0.20 deg	35.48 deg
1850(MHz)	14.08 dB	-0.20 deg	34.97 deg	13.97 dB	-0.40 deg	34.75 deg
1875(MHz)	14.51 dB	-0.40 deg	34.12 deg	14.40 dB	-0.60 deg	34.01 deg
1900(MHz)	14.24 dB	-0.60 deg	34.20 deg	14.13 dB	-0.80 deg	34.01 deg
1925(MHz)	14.67 dB	-0.80 deg	32.54 deg	14.55 dB	-0.80 deg	32.42 deg
1950(MHz)	14.76 dB	-0.80 deg	32.89 deg	14.62 dB	-1.00 deg	32.73 deg
1975(MHz)	14.13 dB	-1.00 deg	32.47 deg	14.00 dB	-1.20 deg	32.33 deg
2000(MHz)	14.84 dB	-1.20 deg	32.54 deg	14.71 dB	-1.20 deg	32.31 deg
2025(MHz)	14.87 dB	-1.00 deg	31.06 deg	14.73 dB	-1.20 deg	31.05 deg
2050(MHz)	14.60 dB	-1.20 deg	32.07 deg	14.45 dB	-1.40 deg	31.98 deg
2075(MHz)	15.44 dB	-1.20 deg	30.30 deg	15.30 dB	-1.20 deg	30.13 deg
2100(MHz)	14.90 dB	-1.20 deg	30.95 deg	14.77 dB	-1.40 deg	30.97 deg
2125(MHz)	14.56 dB	-1.20 deg	30.56 deg	14.41 dB	-1.20 deg	30.34 deg
2150(MHz)	14.98 dB	-1.00 deg	30.50 deg	14.84 dB	-1.20 deg	30.36 deg
2175(MHz)	15.13 dB	-1.00 deg	29.84 deg	15.00 dB	-1.00 deg	29.56 deg
2200(MHz)	15.07 dB	-0.80 deg	29.96 deg	14.95 dB	-1.00 deg	29.64 deg
2225(MHz)	15.30 dB	-1.00 deg	30.02 deg	15.14 dB	-1.20 deg	29.71 deg
2250(MHz)	15.16 dB	-0.60 deg	29.52 deg	15.01 dB	-0.80 deg	28.99 deg
2275(MHz)	13.95 dB	-0.80 deg	29.99 deg	13.81 dB	-1.00 deg	29.82 deg
2300(MHz)	14.71 dB	-0.60 deg	29.37 deg	14.55 dB	-0.60 deg	28.78 deg
2325(MHz)	14.65 dB	-0.60 deg	28.93 deg	14.49 dB	-0.80 deg	28.66 deg
2350(MHz)	14.47 dB	-0.40 deg	29.18 deg	14.30 dB	-0.60 deg	28.62 deg
2375(MHz)	14.75 dB	-0.20 deg	28.36 deg	14.58 dB	-0.20 deg	27.89 deg

2400(MHz)	14.57 dB	-0.20 deg	29.36 deg	14.38 dB	-0.20 deg	28.92 deg
2425(MHz)	14.12 dB	0.20 deg	27.05 deg	13.94 dB	0.00 deg	26.24 deg
2450(MHz)	14.26 dB	0.20 deg	28.16 deg	14.07 dB	0.20 deg	27.71 deg
2475(MHz)	14.18 dB	0.40 deg	28.35 deg	13.94 dB	0.40 deg	27.67 deg
2500(MHz)	14.06 dB	0.60 deg	27.61 deg	13.86 dB	0.60 deg	27.07 deg
2525(MHz)	13.87 dB	0.80 deg	28.42 deg	13.64 dB	0.80 deg	28.02 deg
2550(MHz)	13.60 dB	1.00 deg	27.18 deg	13.39 dB	1.00 deg	26.78 deg
2575(MHz)	12.44 dB	1.00 deg	28.44 deg	12.22 dB	1.00 deg	28.45 deg
2600(MHz)	12.47 dB	1.00 deg	27.42 deg	12.28 dB	1.00 deg	27.24 deg
2625(MHz)	12.61 dB	1.20 deg	28.26 deg	12.45 dB	1.20 deg	28.29 deg
2650(MHz)	11.78 dB	0.80 deg	29.75 deg	11.58 dB	0.80 deg	30.00 deg
2675(MHz)	12.13 dB	0.40 deg	30.21 deg	11.97 dB	0.20 deg	30.19 deg
2700(MHz)	12.09 dB	0.40 deg	32.81 deg	11.92 dB	0.00 deg	32.61 deg
2725(MHz)	10.84 dB	0.00 deg	34.47 deg	10.63 dB	-0.40 deg	33.23 deg
2750(MHz)	9.88 dB	0.20 deg	37.99 deg	9.65 dB	-1.00 deg	36.44 deg
2775(MHz)	9.12 dB	1.00 deg	40.90 deg	8.87 dB	-0.40 deg	38.87 deg
2800(MHz)	9.25 dB	1.00 deg	40.78 deg	9.02 dB	-1.20 deg	38.97 deg
2825(MHz)	10.31 dB	1.40 deg	39.26 deg	9.99 dB	-1.40 deg	38.00 deg
2850(MHz)	10.59 dB	0.60 deg	35.26 deg	10.18 dB	-1.00 deg	34.51 deg
2875(MHz)	9.51 dB	2.40 deg	32.63 deg	9.05 dB	1.80 deg	32.62 deg
2900(MHz)	8.94 dB	4.80 deg	29.26 deg	8.52 dB	4.80 deg	28.92 deg
2925(MHz)	9.44 dB	5.40 deg	25.59 deg	9.04 dB	5.40 deg	25.38 deg
2950(MHz)	9.95 dB	3.40 deg	24.08 deg	9.55 dB	3.40 deg	23.97 deg
2975(MHz)	9.74 dB	1.20 deg	23.63 deg	9.47 dB	1.20 deg	23.74 deg
3000(MHz)	7.15 dB	-1.80 deg	25.17 deg	7.03 dB	-1.80 deg	25.49 deg

These results provide a comprehensive breakdown of the antenna's performance and show the reduction in gain before 1725MHz and after 2725MHz, bounds which correlate with the observed breakdown of the pattern outside of that frequency range. This will be the considered the operating range of this array. Below are more pertinent figures for the MONGOOSE array's performance.

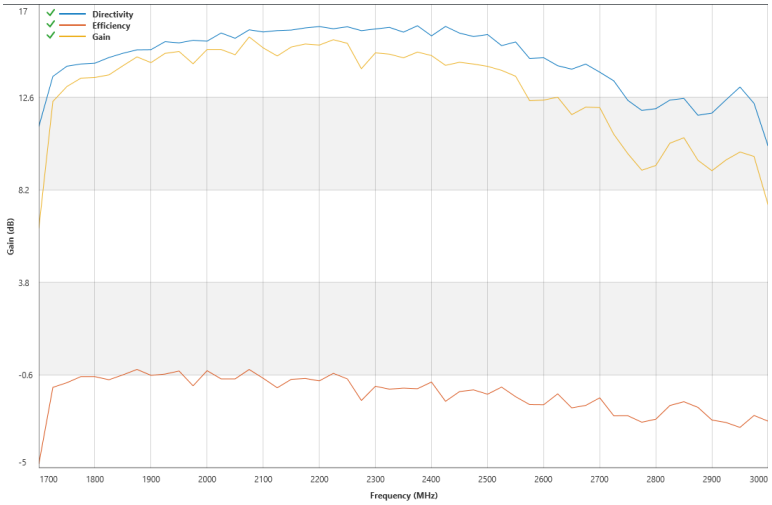

Figure 12 Directivity, Efficiency, Gain over Frequency

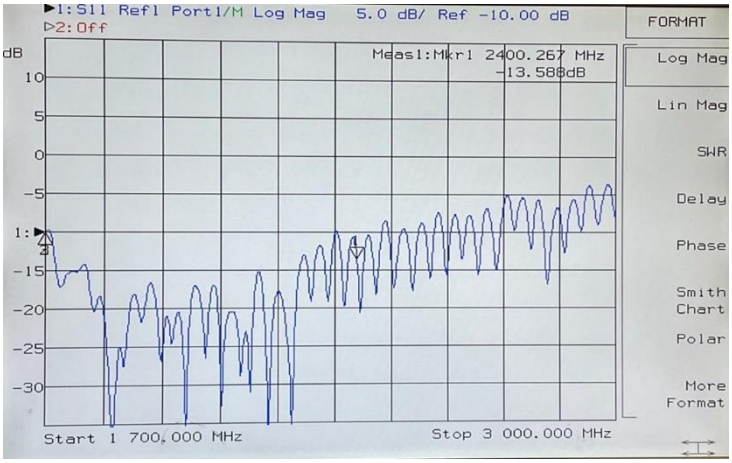

Figure 13 Return Loss for MONGOOSE Array

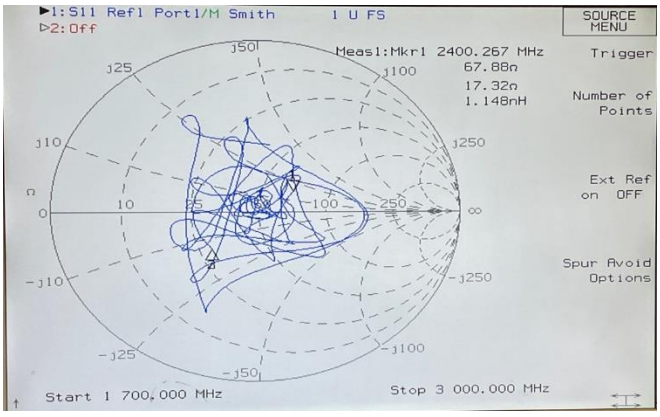

Figure 14 Intrinsic Impedance Smith Chart for MONGOOSE Array

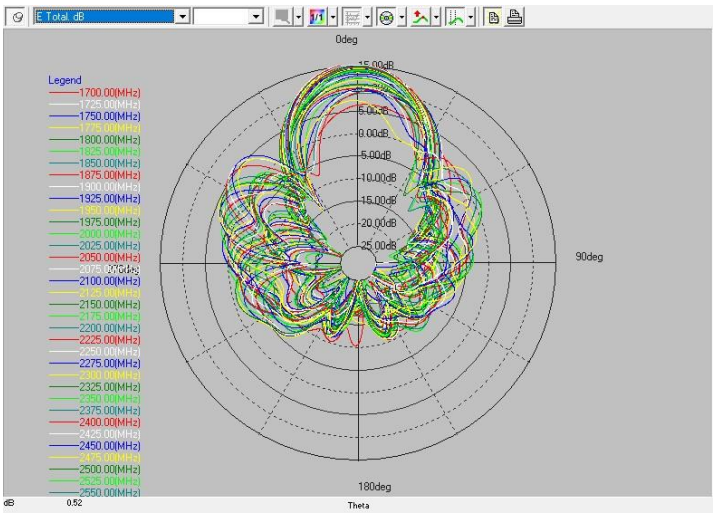

Figure 15 2D Radiation Patterns for All Test Frequencies (1700MHz – 3000MHz, 25MHz Step)

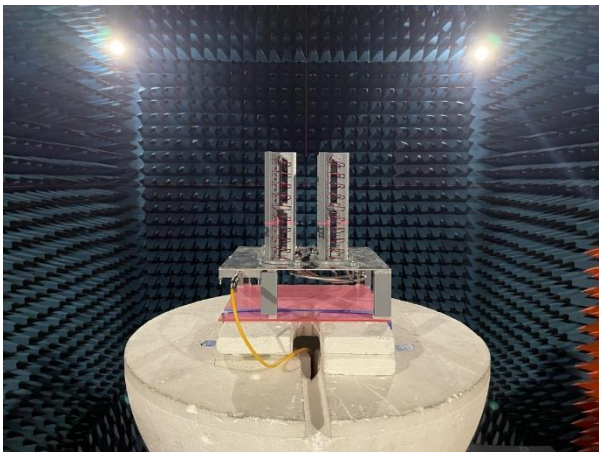

Figure 15 MONGOOSE Array mounted in SG64. Axes: X-right Y-into page Z-up

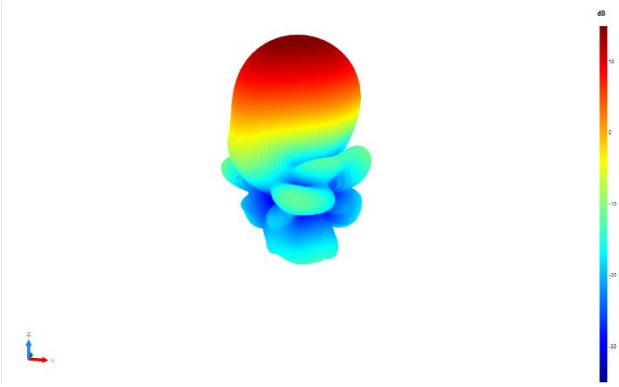

Figure 16 Measured Radiation Pattern at 2.175 GHz

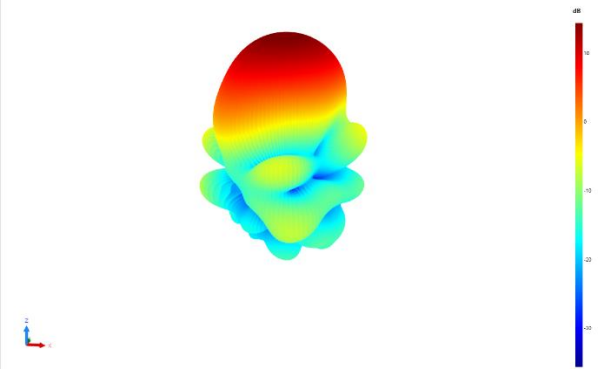

Figure 17 Measured Radiation Pattern at 2.4 GHz

Conclusions

The antenna array functions well within a bandwidth of 1.725 to 2.725 GHz providing a total bandwidth of 1 GHz. Designed with a broad bandwidth in mind, the antenna performs well at common frequencies such as 2.4 GHz, with a rate of 80% efficiency and peak efficiency of 93% occurring at 2.175 GHz. At peak efficiency, the array demonstrates a 14.57 dBi boresight gain at 2.4 GHz. This is shy of the initial goal at 20 dBi, but within range of standard passive satcom antennas. The design, build and testing process showed that results may be able to budge closer to desired gain and additional work is needed to show that 20+ dBi can be achieved with the array of four antennas. As it currently stands, arrays would need more modification to achieve desired gain, although the single helix antenna design matches closely with the initial math and simulations, demonstrating the efficacy of such an antenna design. Future work should address issues such as path losses from each antenna cable, phase matching, microstrip construction, and physical impairments due to support structure design. These losses are due to human handmade device construction and could not be included in simulations, proving the need for more development with the actual device.

Suggestions for Future Work

Phase matching may account for some gain losses. Helices are traveling wave antennas, meaning that their radiation is directly created by the current traveling through the element wire. This also means that small differences in wire length between elements can result in a phase difference proportional to ratio of the difference and the wavelength. This could also explain the higher gain lower in the band where the wavelength is longer and the small wire length differences would impact the phase difference less. We were also unable to quantify phase differences between the paths of the RF power splitter, which could be another source of error. The splitter datasheet indicates a phase shift of less than 4 degrees.

Other improvements could be made such as the design of a PCB corporate feed network that combines the ground plane, power splitter, and matching strips into a single solid-state PCB.

Additionally, transmission and reception capabilities should be tested with message signals as final proof of design. The design, build, and test cycle does well to encourage these areas of work when faced with nonideal conditions and benefits the overall device creation process. Device improvements over the development period indicate there is still room for improvement in design and construction that may yield fruitful results.